Engineering Notes

Flight Control Law Using Composite Nonlinear Feedback Technique for a Mars Airplane

Yanbin Liu[*]
Nanjing University of Aeronautics and Astronautics, 210016 Nanjing, People's Republic of China
Kemao Peng[†]
National University of Singapore, Singapore 117508, Republic of Singapore
Yuping Lu[‡]
Nanjing University of Aeronautics and Astronautics, 210016 Nanjing, People's Republic of China
and
Ben M. Chen[§]
National University of Singapore, Singapore 117576, Republic of Singapore

Nomenclature

$\bar{\beta}$	=	propulsive coefficient
β_c	=	control input concerning thrust
C_D	=	drag coefficient
C_L	=	lift coefficient
$C_{\bar{L}}$	=	roll moment coefficient
C_M	=	pitch moment coefficient
C_N	=	yaw moment coefficient
C_Y	=	lateral force coefficient
δ_a	=	aileron deflection angle, rad
δ_e	=	elevator deflection angle, rad
δ_r	=	rudder deflection angle, rad

I. Introduction

DESIGNING an aircraft for Mars presents a very challenging task that involves flying through the Martian atmosphere, which has low pressure and density. Such an extraterrestrial aircraft should have many flight characteristics that differ from that of a typical Earth aircraft [1]. On the one hand, the thin atmosphere flight of a Mars airplane tends to have a very low aerodynamic damping in combination with high subsonic Mach numbers and very low Reynolds numbers, thereby leading to unfavorable control results [2]. In particular, actuator saturation easily occurs as a result of the low atmosphere density and small assembled wing area. On the other hand, Martian atmospheric conditions may vary 20% or more from these nominal values as a result of the surface wind and different location [3]. Therefore, steady tracking performance, transient response property, and system robustness are critical for flight control to accomplish the challenging deep-space exploration task under a high-subsonic low-Reynolds-number regime.

For a Mars airplane, Hjartarson et al. [4] presented a blend of H_∞ and proportional–integral controller to stabilize the aircraft under complicated flight conditions. Similarly, Bhattacharya et al. [5] provided the framework of the general mixed sensitivity H_∞ control to solve the longitudinal reference tracking problem, and the results showed that the designed controller can tolerate a potential 70% plant uncertainty. Brown et al. [6] dealt with the work on the design, construction, and flight testing of a Mars airplane demonstrator to show the system stability, control, and performance of the proposed Mars airplane. Nevertheless, these methods give more attention to system robustness than to transient performance, which contributes to the overall control qualities [7]. To this end, the present study uses the composite nonlinear feedback (CNF) technique proposed by Chen et al. [8] to design a novel flight control law for a Mars airplane. This controller consists of a linear and a nonlinear feedback control law without any switching element, such that the CNF design is capable of capturing the time-optimal maneuver in asymptotically tracking situations [9]. Thus, the proposed controller considers integrated control performances consisting of fast settling time, small overshoot, and strong robustness in the unknown Martian environment.

The remainder of this paper is organized as follows. Section II explores the longitudinal and lateral/directional model transformation of the Mars airplane using feedback linearization theory. Section III considers the design problem of the flight control law by applying the CNF technique and analyzes and proves accordingly the system stability and robustness. Section IV provides an illustrative example of the proposed controller for a nonlinear model of the Mars airplane, in which the tracking performances are compared using the CNF control and pole displacement method.

II. Control-Oriented Model Transformation of a Mars Airplane

The task of the Aerial Regional-Scale Environmental Survey (ARES) is to obtain scientific data on Mars that cannot be acquired from either ground vehicles or orbiters [3]. However, in contrast to the Earth's atmosphere, the Martian atmosphere is spare and composed of carbon dioxide. Thus, the Mars atmospheric model must be identified first before building a model of a Mars airplane. In particular, the Mars global reference atmospheric model (Mars-GRAM) can describe the density variations for a given altitude in relation to solar longitude [10]. On this basis, this work adopts the simplified atmospheric model in the simulation [4]. Furthermore, the model properties of an ARES airplane, which consists of the aerodynamic data and geometrical parameters in [5], are used to validate the effectiveness of the proposed methods.

A. Longitudinal Model and State Transformation

We assume that the coupling relations between the longitudinal and lateral/directional modes are weak as a result of the relative small aerodynamic forces as well as the anticipated exploration task, which ensures that the Mars airplane maintains the level flight to acquire the valuable data from the planet's surface. To this end, the nonlinear longitudinal model of the Mars airplane is depicted in [11]

*Associate Professor, College of Astronautics.
†Senior Research Scientist, Temasek Laboratories.
‡Professor, College of Automation Engineering.
§Professor, Department of Electrical and Computer Engineering.

$$\begin{cases} \dot{V} = \frac{T \cos \alpha - D}{m} - g \sin \gamma \\ \dot{\gamma} = \frac{L + \frac{T}{m} \sin \alpha}{mV} - \frac{g \cos \gamma}{V} \\ \dot{q} = M_y / I_y \\ \dot{\alpha} = q - \dot{\gamma} \\ \dot{h} = V \sin \gamma \end{cases} \quad (1)$$

In Eq. (1), V, γ, q, α, and h are the airspeed, flight path angle, pitch rate, angle of attack, and altitude, respectively; m and I_y denote the mass and pitch moment of inertia, respectively; and the lift L, drag D, pitch moment M_y, and thrust T determine the flight characteristics of the Mars airplane and are calculated by $L = 0.5\rho V^2 S C_L$, $D = 0.5\rho V^2 S C_D$, $M_y = 0.5\rho V^2 S \bar{c} C_M$, and $T = T_M \bar{\beta}$, where $\bar{c}$, S, and T_M denote the mean aerodynamic chord, wing area, and maximum thrust, respectively. Additionally, the propulsive model is considered to be $\ddot{\beta} = -2\xi\varpi\dot{\beta} - \varpi^2\beta + \varpi^2\beta_c$, where ϖ and ξ denote the frequency and damping ratio of the propulsive system, respectively. For simplicity, the air density ρ and acceleration due to gravity, g, are used as the function of flight height.

For Eq. (1), the presence of a nonminimum phase zero in the transfer function $\Delta\gamma/\Delta\delta_e$ is caused by the lift corresponding to the elevator deflection [12]. In particular, $Z_{\delta_e} = -(1/m)(\partial L/\partial \delta_e)$ is very small for the Mars airplane because of the very low atmospheric density, such that this nonminimum phase zero is located to the far right. Meanwhile, a lag is apparent between the flight path and pitch angles because the Martain atmosphere density slope, along with altitude, is relatively low [13]. On this basis, this work ignores the influence of the lift and drag corresponding to the elevator deflection on the control design, and the corresponding aerodynamic coefficients of the longitudinal model in Eq. (1) are expressed by

$$\begin{cases} C_L = f_L(\alpha) \\ C_D = f_D(\alpha) \\ C_M = f_{M_y}(\alpha, q) + f_{\delta_e}\delta_e \end{cases} \quad (2)$$

where f_{δ_e} denotes the moment coefficient with respect to the elevator. Furthermore, the nonlinear longitudinal model of the Mars airplane is rewritten as

$$\begin{cases} \dot{X} = f(X) + G(X)U \\ y = H(X) \end{cases} \quad (3)$$

where the flight state vector X is defined as $X = [V, \gamma, \alpha, \bar{\beta}, h]'$; the control input vector U is considered to be $U = [\delta_e, \beta_c]'$; and the output vector is given as $y = [V, h]'$. In addition, $G = [g_\delta, g_\beta]'$ represents the input matrix, whereas f, H, g_δ, and g_β denote the vectors determined by the longitudinal airplane model in Eq. (1). Therefore, this airplane model can be regarded as a two-input/two-output nonlinear system.

Consider the nonlinear model in Eq. (3); we assume that f, H, g_δ, and g_β are smooth. In this case, the third-order derivative of V is expressed by [14]

$$V^{(3)} = V_0^{(3)} + b_{11}\delta_e + b_{12}\beta_c \quad (4)$$

where $V_0^{(3)}$, b_{11}, and b_{12} are the resulting model parameters regarding the velocity, and they are determined by the standard form of the feedback linearization. For this reason, the Lie derivative of function H along f is adopted by

$$L_f H = \frac{\partial H}{\partial X} f(X) \quad (5)$$

Similarly, $L_f^k H (k = 2, 3, \ldots)$ indicate the higher-order Lie derivatives, whereas $L_{\delta_e} H$ is used to represent the Lie derivative of the function H corresponding to δ_e. Following the result of [14], we have $L_f V = \dot{V}$, $L_f^2 V = \ddot{V}$, $L_f^3 V = V_0^{(3)}$, $L_{g_\delta} L_f^2 V = b_{11}$, and $L_{g_\beta} L_f^2 V = b_{12}$, such that the three time derivatives of V depend explicitly on the control inputs δ_e and β_c. The same Lie derivative operation is in turn conducted for h, yielding

$$h^{(4)} = h_0^{(4)} + b_{21}\delta_e + b_{22}\beta_c \quad (6)$$

where $h_0^{(4)}$, b_{21}, and b_{22} denote the resulting model parameters regarding the altitude. Furthermore, considering $L_f h = \dot{h}$, $L_f^2 h = \ddot{h}$, $L_f^3 h = h^{(3)}$, $L_f^4 h = h_0^{(4)}$, $L_{g_\delta} L_f^3 h = b_{21}$, and $L_{g_\beta} L_f^3 h = b_{22}$, we simultaneously define $X_V = [z_1, z_2, z_3]' = [V, L_f V, L_f^2 V]'$, $X_h = [z_4, z_5, z_6, z_7]' = [h, L_f h, L_f^2 h, L_f^3 h]'$, and $z = [X_V, X_h]'$. The equivalent model corresponding to the nonlinear model [Eq. (1)] is then given by [15]

$$\begin{bmatrix} V^{(3)} \\ h^{(4)} \end{bmatrix} = \begin{bmatrix} V_0^{(3)} \\ h_0^{(4)} \end{bmatrix} + \begin{bmatrix} b_{11}(z) & b_{12}(z) \\ b_{21}(z) & b_{22}(z) \end{bmatrix} \begin{bmatrix} \delta_e \\ \beta_c \end{bmatrix} = F_0 + B(z)U \quad (7)$$

According to Eq. (7), we know that the resulting model has a full vector relative degree $r = 7$, and this indicates that the control goal is to guarantee system stability for Eq. (7) because there is no zero dynamics for the nonlinear model of Eq. (1). In other words, the nonlinear model is completely linearized if Eq. (2) is satisfied [16] because the relative degree is equal to the order number of the nonlinear model.

B. Lateral/Directional Model and State Transformation

For the given flight point, the lateral/directional model of a Mars airplane is simplified as

$$\begin{cases} mV\dot{\beta} = Y - mV(-p \sin \alpha + r \cos \alpha) \\ \dot{\phi} = p + (r \cos \phi + q \sin \phi) \tan \theta \\ \dot{\psi} = \frac{1}{\cos \theta}(r \cos \phi + q \sin \phi) \\ \dot{p} = \frac{\bar{L}}{I_x} \\ \dot{r} = \frac{N}{I_z} \end{cases} \quad (8)$$

In Eq. (8), β, ϕ, ψ, p, and r denote the sideslip angle, roll angle, yaw angle, roll rate, and yaw rate, respectively; and I_x and I_z are the roll moment of inertia and yaw moment of inertia, respectively. The lateral force Y, roll moment $\bar{L}$, and yaw moment N are computed by $Y = 0.5\rho V^2 S C_Y$, $\bar{L} = 0.5\rho V^2 S b C_{\bar{L}}$, and $N = 0.5\rho V^2 S b C_N$, where b is the wingspan. Furthermore, we assume that C_Y, $C_{\bar{L}}$, and C_N are determined by

$$\begin{cases} C_Y = f_Y \beta \\ C_{\bar{L}} = f_{M_L} + f_{\delta_a}\delta_a \\ C_N = f_{M_N} + f_{\delta_r}\delta_r \end{cases} \quad (9)$$

where f_Y, f_{M_L}, and f_{M_N} are the model coefficients with respect to β; and f_{δ_a} and f_{δ_r} are the lateral/directional nonlinear aerodynamic parameters related to δ_a and δ_r. Afterward, taking the second derivation of β and ψ, we have

$$\begin{cases} \ddot{\psi} = \ddot{\psi}_0 + \frac{0.5 \cos \phi \rho V^2 S b f_{\delta_r}}{\cos \theta I_z}\delta_r \\ \ddot{\beta} = \ddot{\beta}_0 + \frac{0.5 \sin \alpha \rho V^2 S b f_{\delta_a}}{I_x}\delta_a - \frac{0.5 \cos \alpha \rho V^2 S b f_{\delta_r}}{I_z}\delta_r \end{cases} \quad (10)$$

where

$$\begin{cases} \ddot{\psi}_0 = \frac{(q \cos \phi - r \sin \phi)(p + r \cos \phi \tan \theta + q \sin \phi \tan \theta)}{\cos \theta} + \frac{0.5 \cos \phi \rho V^2 S b f_{M_N}}{\cos \theta I_z} \\ \ddot{\beta}_0 = \frac{0.5\rho V^2 S f_Y \dot{\beta}}{mV} + \frac{0.5 \sin \alpha \rho V^2 S b f_{M_L}}{I_x} - \frac{0.5 \cos \alpha \rho V^2 S b f_{M_N}}{I_z} \end{cases} \quad (11)$$

According to Eq. (11), we know that the nonlinear lateral/directional model can be linearized if the longitudinal states are fixed under the assumption that the coupling relations between the longitudinal and lateral/directional modes are neglected.

Based on the equivalent models in Eqs. (7) and (10), the control law using the CNF technique can be designed accordingly to

guarantee the satisfactory control performances involving fast settling time, small overshoot, and strong robustness.

III.   Flight Control Law Design Using Composite Nonlinear Feedback Technique

The design goal of this section is to obtain a flight control law for the Mars airplane using the CNF technique, such that the resulting closed-loop system remains stable and the system outputs can rapidly track the given commands. Without loss of generality, the equivalent model of the longitudinal model in Eq. (7) is regarded as the control design object; thus, the step-by-step control design procedure using the CNF technique is as follows.

Step 1: Design a linear feedback law [8]

$$\begin{cases} U_{VL} = F_V X_V + G_V V_c \\ U_{hL} = F_h X_h + G_h h_c \end{cases} \qquad (12)$$

for the equivalent form of Eq. (7)

$$\begin{cases} \dot{X}_V = A_V X_V + B_V \Upsilon_V, & Y_V = V = C_V X_V \\ \dot{X}_h = A_h X_h + B_h \Upsilon_h, & Y_h = h = C_h X_h \end{cases} \qquad (13)$$

where $\Upsilon_V = V^{(3)}$, $\Upsilon_h = h^{(4)}$, $G_V = -[C_V(A_V + B_V F_V)^{-1} B_V]^{-1}$, and $G_h = -[C_h(A_h + B_h F_h)^{-1} B_h]^{-1}$. Additionally, V_c and h_c are the step commands with regard to the flight velocity and altitude, whereas $F_V = [f_{V1}, f_{V2}, f_{V3}]$ and $F_h = [f_{h1}, f_{h2}, f_{h3}, f_{h4}]$ indicate the resulting vectors, as determined by the next step.

Step 2: Design a nonlinear feedback part

$$\begin{cases} U_{VN} = \rho_V B_V' P_V (X_V - X_{Ve}) \\ U_{hN} = \rho_h B_h' P_h (X_h - X_{he}) \end{cases} \qquad (14)$$

where $X_{Ve} = G_{Ve} V_c = -(A_V + B_V F_V)^{-1} B_V G_V V_c$; $X_{he} = G_{he} h_c = -(A_h + B_h F_h)^{-1} B_h G_h h_c$; and P_V and P_h are determined by

$$\begin{cases} P_V A_V + A_V' P_V - P_V B_V R_V^{-1} B_V' P_V + Q_V = 0 \\ P_h A_h + A_h' P_h - P_h B_h R_h^{-1} B_h' P_h + Q_h = 0 \end{cases} \qquad (15)$$

where Q_V and Q_h are the given positive-definite matrices; $R_V > 0$ and $R_h > 0$ indicate the selected scalars; and ρ_V and ρ_h denote the designed nonpositive nonlinear terms to improve the tracking performance. Furthermore, F_V and F_h in Eq. (12) are decided by

$$\begin{cases} F_V = -R_V^{-1} B_V' P_V \\ F_h = -R_h^{-1} B_h' P_h \end{cases} \qquad (16)$$

Step 3: The linear feedback control law and nonlinear feedback portion are combined to constitute the CNF control law

$$\begin{cases} \Upsilon_V = U_{VL} + U_{VN} \\ \Upsilon_h = U_{hL} + U_{hN} \end{cases} \qquad (17)$$

Step 4: If the matrix B is full rank, the flight control law is obtained as

$$\begin{bmatrix} \beta_c \\ \delta_e \end{bmatrix} = \begin{bmatrix} b_{11} & b_{12} \\ b_{21} & b_{22} \end{bmatrix}^{-1} \left(\begin{bmatrix} \Upsilon_V \\ \Upsilon_h \end{bmatrix} - \begin{bmatrix} V_0^{(3)} \\ h_0^{(4)} \end{bmatrix} \right) \qquad (18)$$

Furthermore, we consider the input saturation for the nonlinear airplane model; the control design goal is to develop a flight control law using CNF so that the outputs $y = [V, h]'$ can asymptotically track the step references $y_c = [V_c, h_c]'$. First, the equivalent model in Eq. (7) is reshaped as

$$\begin{cases} \dot{z} = A_z z + B_z v_z, & v_z = F_0(z) + B(z) \, \mathrm{sat}(U) \\ y = C_z z \end{cases} \qquad (19)$$

where $U = [u_V, u_h]' = [\beta_c, \delta_e]'$, and "sat" represents the saturation function. The resulting system matrices denote $A_z = \mathrm{diag}(A_V, A_h)$, $B_z = \mathrm{diag}(B_V, B_h)$, and $C_z = \mathrm{diag}(C_V, C_h)$.

Accordingly, the flight control law using CNF in Eq. (18) can be reshaped as follows:

$$U = B(z)^{-1}[(F_z z + G_z y_c) + \rho_{zz} B_z' P_z(z - G_{ze} y_c) - F_0(z)] \qquad (20)$$

where $P_z = \mathrm{diag}(P_V, P_h)$, $F_z = \mathrm{diag}(F_V, F_h)$, $G_z = \mathrm{diag}(G_V, G_h)$, $\rho_{zz} = \mathrm{diag}(\rho_V, \rho_h)$, and $G_{ze} = \mathrm{diag}(G_{Ve}, G_{he})$. Substituting Eqs. (15) and (20), we have

$$U = B(z)^{-1}[F_z(z - G_{ze} y_c) - \rho_{zz} R_z F_z(z - G_{ze} y_c) - F_0(z)] \qquad (21)$$

where $R_z = \mathrm{diag}(R_V, R_h)$. Let $\rho_z = I_{zz} - \rho_{zz} R_z$, where I_{zz} is the unity matrix; we obtain

$$U = B(z)^{-1}[\rho_z F_z(z - G_{ze} y_c) - F_0(z)] \qquad (22)$$

Afterward, we assume that there exists a scalar $\mu > 0$, and a set of scalars $\tau_i \in (0, 1)$, $i = V, h$ exist, so that

$$X_{iV} = \{X: X' P_z X \leq \mu\} \Rightarrow \|e_i' B^{-1}(z_t)\| \|F_z X\| \leq (1 - \tau_i) \bar{u}_i \qquad (23)$$

where z_t represents a chosen nominal point; $\bar{u}_i$ denotes the maximum value with respect to the control input; and e_i is a vector in which only the ith element of e_i is 1 and the others are zero. Furthermore, the subsequent theorem is given next.

Theorem 1: Suppose that 1) f, g_δ, g_β, and H in Eq. (3) are smooth vectors on a compact and connected set χ of $\mathbb{R}^n$, and 2) $B(z)$ is invertible at $\forall z \in Z$, in which $z = \Phi(X)$ is nonsingular on χ.

Then, the control law [Eq. (18)] can drive the system outputs $y = [V, h]'$ to asymptotically track the step commands $y_c = [V_c, h_c]'$, if the following are true.

1) There exist a set of scalars, $\tau_i \in (0, 1)$, $i = V, h$ so that

$$\|e_i' B^{-1}(z) F_0(z)\| \leq \tau_i \bar{u}_i, \quad \forall z \in Z \qquad (24)$$

2) $\rho_z = \mathrm{diag}(\rho_{zV}, \rho_{zh})$, and ρ_{zi} is a continuous function for $i = V$, h. Let X_t be a chosen nominal point so that

$$\min(\rho_{zV}, \rho_{zh}) > \frac{1}{2}, \qquad \sigma_{\min}(R_p) > \frac{1}{2}, \quad \forall z \in Z \qquad (25)$$

where $R_p = B(z) B^{-1}(z_t)$, $z_t = \Phi(X_t)$, and $z_t \in Z$. $\sigma_{\min}$ denotes the minimal singular value.

3) Let X_{iV} be the initial value of X. Then, z_{iV} and a step reference y_c satisfy

$$z_{iV} - G_{ze} y_c \in X_{iV}, z_{iV} = \Phi(X_{iV}) \qquad (26)$$

Proof: See Appendix A.

Remark 1: The designed control law for the lateral/directional model is similar to that in Eq. (18) for the Mars airplane, and this topic is not discussed here due to limitations of space. In general, the flight control structure can be built for the Mars airplane using the CNF technique depicted in Fig. 1.

Remark 2: ρ_{zi}, $i = V$, h corresponds to $e_i' y$ so that ρ_{zi} can be designed as a continuous function of the tracking error to automatically and smoothly result in low and high damping ratios to improve the dynamic performance. According to $\rho_z = I_{zz} - \rho_{zz} R_z$, we have

$$\begin{cases} \rho_{zV} = 1 - \rho_V / R_V \\ \rho_{zh} = 1 - \rho_h / R_h \end{cases} \qquad (27)$$
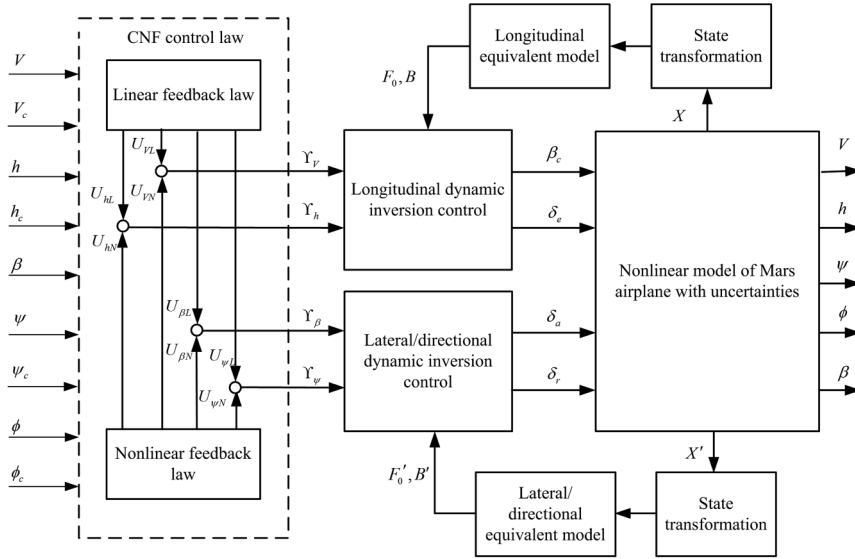
Fig. 1 Flight control structure for Mars airplane using CNF technique.

This shows that Theorem 1 is always satisfied if ρ_V and ρ_h are nonpositive functions, so that the choices of ρ_{zV} and ρ_{zh} can be based on this theorem. A low damping ratio is required to achieve fast rising and regulating time when the tracking error is large. A higher damping ratio is provided to decrease the overshoot when the output reaches the target of a step reference. For instance, the following choices of ρ_V and ρ_h are smooth and nonpositive functions of $e_V = V - V_c$ and $e_h = h - h_c$:

$$\begin{cases} \rho_V = -\varepsilon_V|e^{-\tau_V|e_V|} - e^{-\tau_V|V_0-V_c|}| \\ \rho_h = -\varepsilon_h|e^{-\tau_h|e_h|} - e^{-\tau_h|h_0-h_c|}| \end{cases} \quad (28)$$

where V_0 and h_0 indicate the nominal flight point; and ε_V, ε_h, τ_V, and τ_h are suitable positive scalars that can be chosen in terms of the desired track performances, that is, fast settling time and small overshoot. At the initial response, when the controlled outputs are away from the step commands, the influence of the nonlinear portion are limited because the nonlinear parts are small. By contrast, when the track errors reach the given commands, the nonlinear part becomes effective. Correspondingly, the overshoot of the output response for the Mars airplane decreases accordingly.

Remark 3: The main goal of adding the nonlinear part is to change the damping ratios of the closed-loop system as the outputs approach the step commands [17]. However, the dynamic inversion controller needs some level of robustness to relieve the undesired dynamics caused by model uncertainties [18]. On this basis, the nonlinear gains ρ_V and ρ_h must be discussed, given that they can also improve stability robustness. Considering the model uncertainties ω_V and ω_h and substituting Eqs. (12–18) into Eq. (7), we have

$$\begin{cases} \dot{E}_V = A_{eV}E_V + B_{eV}\rho_V B_V^T P_V E_V + B_{eV}\omega_V \\ \dot{E}_h = A_{eh}E_h + B_{eh}\rho_h B_h^T P_h E_h + B_{eh}\omega_h \end{cases} \quad (29)$$

where

$$\begin{cases} E_V = [e_V, \dot{e}_V, \ddot{e}_V]', & A_{eV} = (A_V + B_V F_V), & B_{eV} = B_V \\ E_h = [e_h, \dot{e}_h, \ddot{e}_h, e_h^{(3)}]', & A_{eh} = (A_h + B_h F_h), & B_{eh} = B_h \end{cases} \quad (30)$$

Furthermore, a Lyapunov function is defined:

$$\Gamma_L = \Gamma_V + \Gamma_h = \frac{1}{2}E_h'P_h E_h + \frac{1}{2}E_V'P_V E_V \quad (31)$$

The time derivative of Γ_V is determined by

$$\dot{\Gamma}_V = E_V'[(A_V + B_V F_V)'P_V + P_V(A_V + B_V F_V)]E_V$$
$$+ 2\rho_V E_V'P_V B_V B_V'P_V E_V + (B_{eV}'P_V E_V + E_V'P_V B_{eV})\omega_V$$
$$= -E_V'Q_V E_V - (\gamma_V E_V'P_V B_V - \omega_V/\gamma_V)^2 + \omega_V^2/\gamma_V^2$$
$$\leq -E_V'Q_V E_V + \omega_V^2/\gamma_V^2 \quad (32)$$

where $\gamma_V^2 = -2\rho_V + R_V^{-1}$, and integrating the preceding inequality from $t = 0$ to T_0 yields

$$\Gamma_V(T_0) + \int_0^{T_0} \|E_V(t)\|_{Q_V}^2 \, dt \leq \Gamma_V(0) + \gamma_V^{-2}\int_0^{T_0} \|\omega_V\|^2 \, dt,$$
$$0 \leq T_0 < \infty \quad (33)$$

The preceding equation shows that an H^∞ performance is achieved [19]. From Γ_V in Eq. (33), we know that $E_V \in \Omega_V \Delta = \{E_V|E_V'P_V E_V \leq 2\Gamma_V(0) + M_V^2/\gamma_V^2\}$, so that the closed system can maintain stability robustness. Furthermore, Eq. (29) is reshaped as

$$\dot{E}_V = (A_V + B_V F_V + \rho_V B_{eV}B_V^T P_V)E_V + B_{eV}\omega_V \quad (34)$$

Based on Eq. (34), it is clear that eigenvalues of the closed-loop system can be affected by the function ρ_V. Under such a circumstance, the classical feedback control concept can be applied, where the auxiliary system $G_{auxV}(s)$ for E_V is defined as [8]

$$G_{auxV}(s) = C_{aux}(sI - A_{aux})^{-1}B_{aux} = B_V'P_V(sI - A_V - B_V F)^{-1}B_V \quad (35)$$

Following the result of [8], the poles of the closed-loop system for E_V in Eq. (34) approach the locations of the invariant zeros of $G_{auxV}(s)$ as $|\rho_V|$ becomes larger and larger. In other words, $|\rho_V|$ affects the poles of the closed-loop system of Eq. (34) in relation to the stability of the closed-loop system. The same analysis process is in turn conducted for Γ_h in Eq. (31). As a result, the proposed control law using the CNF technique not only ensures the stability of the closed-loop system but also suppresses the effect of uncertainties.

IV. Illustrative Example

This study uses the airplane model with respect to the ARES configuration to validate the feasibility of the presented control law [5]. Using the least-squares fitting methods for these aerodynamic coefficients in [5], the resulting aerodynamic expressions are approximately obtained by

$$
\begin{cases}
C_L = 5.0512\alpha + 0.2346 \\
C_D = 2.3114\alpha^2 - 0.0096\alpha + 0.0364 \\
C_Y = -0.2578\beta \\
C_{\bar{L}} = 0.0688\beta - 0.1490\delta_a \\
C_M = 1.9091\alpha^2 - 0.5638\alpha + 0.0401 - 0.8595\delta_e \\
C_N = 0.0859\beta - 0.0802\delta_r
\end{cases}
\tag{36}
$$

The flight control law with CNF is applied for the nonlinear model of the Mars airplane with input saturation to demonstrate the improvement of the transient performance relative to that with the control law using the pole displacement method. We choose R_V and R_h as the identity matrix. Afterward, the nonlinear gain functions in Eq. (28) are selected as $\varepsilon_V = \varepsilon_h = 10$ and $\tau_V = \tau_h = 0.2$.

In the simulation, we account for the comparative results between the controller using CNF and that using the pole placement method provided in [20]. This controller is based on the pole placement method and Lyapnouv equation to ensure the Hurwitz stability. When passing through 200 s, the response curves are acquired corresponding to $h_c = h_0 + \Delta h_c = 2540$ m, $V_c = V_0 + \Delta V_c = 230.06$ m/s,
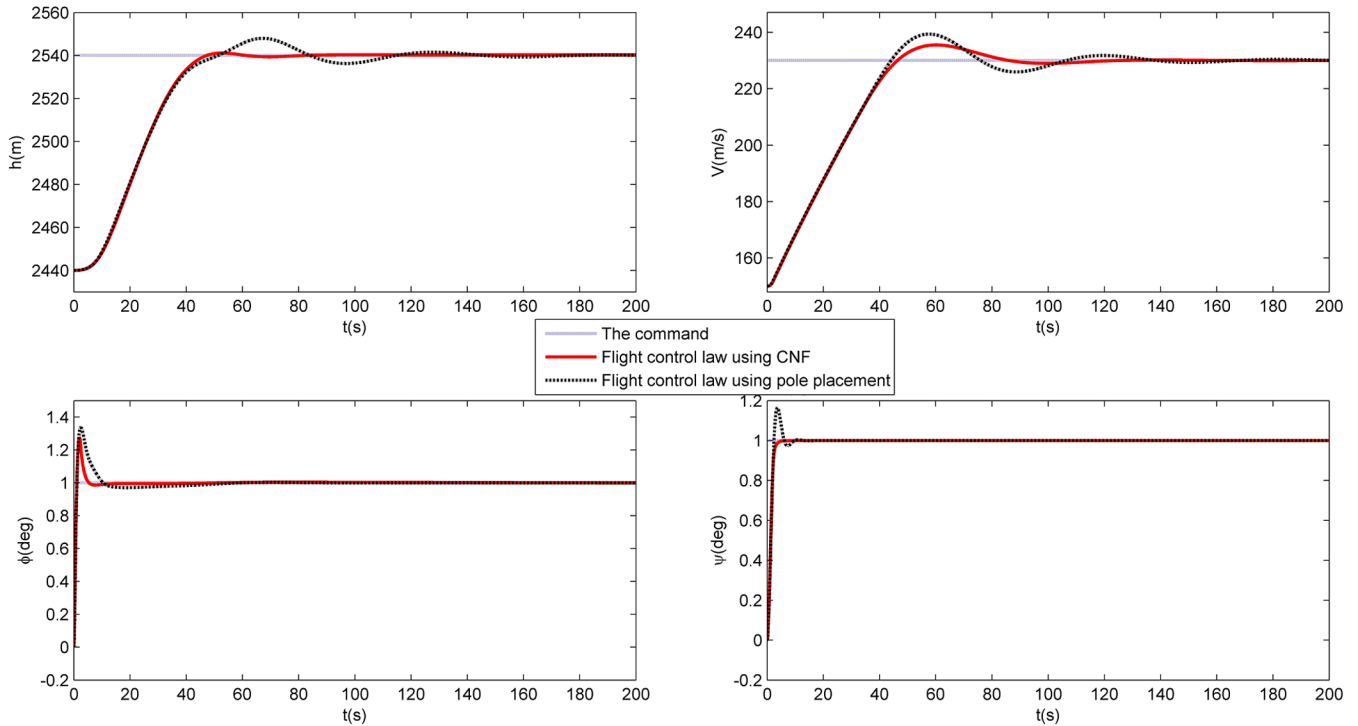
Fig. 2   Contrast track curves between using CNF and using pole placement.
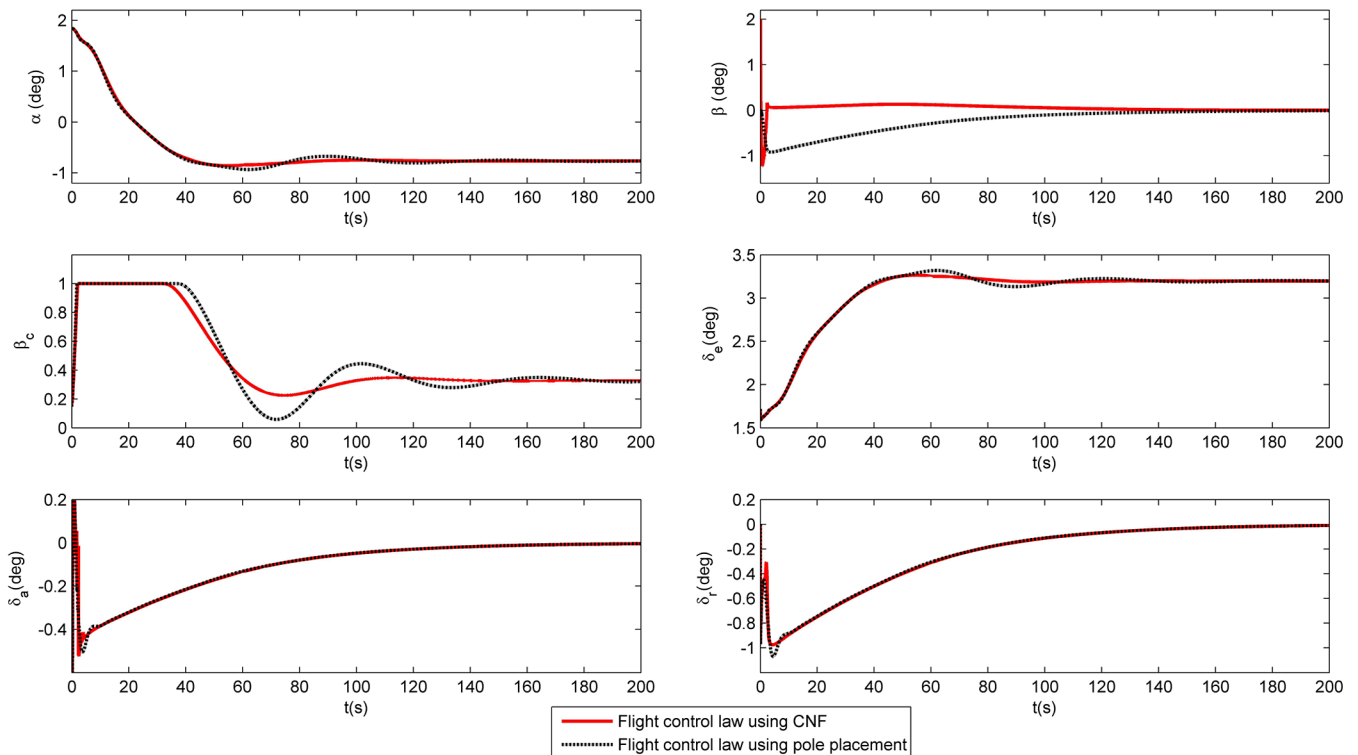
Fig. 3   Flight states and control inputs between using CNF and using pole placement.

$\phi_c = \phi_0 + \Delta\phi_c = 1$ deg, and $\psi_c = \psi_0 + \Delta\psi_c = 1$ deg where $V_0 = 150.06$ m/s, $h_0 = 2440$ m, $\phi_0 = 0$ deg, and $\psi_0 = 0$ deg. They are shown in Figs. 2 and 3.

Figure 2 demonstrates the contrast curves between using CNF and using pole placement. Owing to the nonlinear part of the CNF control law in Eq. (14), the velocity and altitude output can rapidly track the commands signals in contrast to the control law using the pole placement method, including faster settling time and smaller overshoot. Figure 3 shows that the change curves of the angle of attack and control inputs gently return to the anticipated balance values resulting from the control action, whereas the last time of the

control input saturation reduces as the nonlinear part for CNF takes effect. The change curves of the nonlinear gains along with the track errors are provided in Fig. 4.

Figure 4 shows that the nonlinear gains can be regulated to result in a low damping ratio to achieve a fast rising time when large tracking errors exist and a high damping ratio to remove the overshoot caused by the low damping ratio when the track error approaches zero. Furthermore, the dynamic performance indices with regard to the overshoot and settling time are provided in Table 1.

According to Table 1, we know that the dynamic performance indices using the flight control law with CNF are better than those
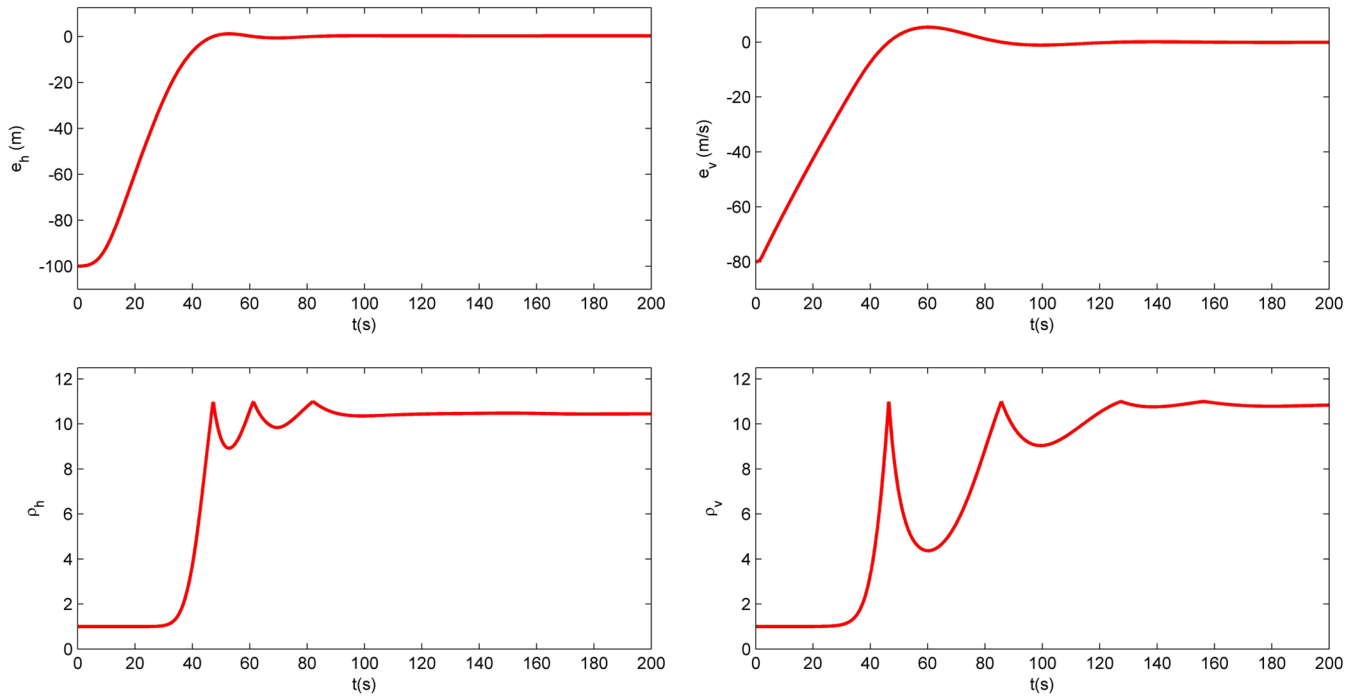
Fig. 4 Change curves of nonlinear gains along with the track errors.
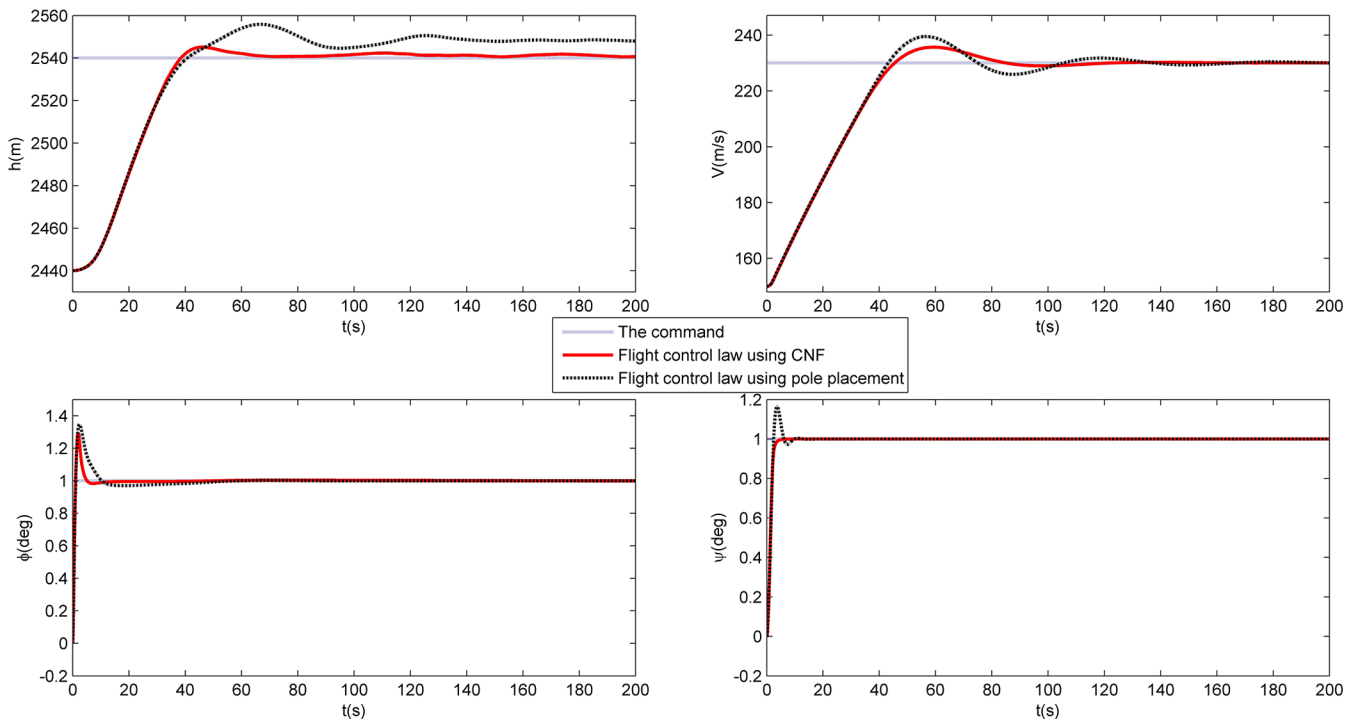
Fig. 5 Track response curves for uncertain model.

Table 1   Dynamic performance indices in the track process

Control modes	Overshoot using CNF, %	Overshoot using pole placement, %	Settling time using CNF, s	Settling time using pole placement, s
Altitude control	1.16	7.99	41.10	75.79
Velocity control	6.85	11.68	69.65	90.94
Roll angle control	28.13	34.35	3.91	8.21
Yaw angle control	5.8e-5	16.65	2.53	5.31

using the pole placement method. For example, settling time decreases dramatically because of the existence of the nonlinear part of CNF. In addition, actual atmospheric conditions on Mars may change 20% or more due to location, season, and time of day [3]. To this end, we further consider the 30% random uncertainties of the aerodynamic forces and the 50% random uncertainties of the aerodynamic moments. When the control law using CNF is applied, the corresponding results are shown in Figs. 5 and 6.

Figures 5 and 6 show that the response results are satisfactory even in the case of the large uncertainties and that the velocity and altitude tracking errors are kept small as the response process enters the steady state. Additionally, the nonlinear gains of CNF can make the designed control law achieve better flight performances. The control inputs also induce the jigger in relation to the random uncertainties, which indicates that the closed system has a satisfactory self-adaptive control ability to suppress uncertain disturbances caused by the existence of the nonlinear gains ρ_V and ρ_h, thereby improving stability robustness. In summary, the CNF technique assists to ameliorate control qualities, including fast settling time, small overshoot, and strong robustness for the Mars airplane.

V.   Conclusions

This study proposes a design method of flight control law using the composite nonlinear feedback technique for the Mars airplane. This proposed control law is further applied to a nonlinear model of a Mars airplane, and the simulation results display that the proposed control law improves the dynamic performance with input saturation. More importantly, the strong robustness of the closed-loop system is ensured for the Mars airplane even while considering large uncertain disturbances.

Appendix: Proof of Theorem 1

Let $\tilde{z} = z - G_{ze}y_c$; then,

$$U = B(z)^{-1}\rho_z F_z \tilde{z} - B(z)^{-1}F_0(z) \tag{A1}$$

When $\tilde{z} \in X_{iV}$, it implies that

$$\|e_i'B^{-1}(z_t)\|\|F_z\tilde{z}\| \le (1 - \tau_i)\bar{u}_i \tag{A2}$$

When $0 < \|\rho_z\| \le \sigma_{\min}(R_p)$, considering Eq. (25), we have

$$\|e_i'B^{-1}(z)\rho_z\| \le \|e_i'B^{-1}(z)\|\|\rho_z\| \le \|e_i'B^{-1}(z)\|\sigma_{\min}(R_p)$$
$$\le \|e_i'B^{-1}(z)R_p\| = \|e_i'B^{-1}(z_t)\| \tag{A3}$$

With Eqs. (23), (A2), and (A3), we have

$$\|e_i'B^{-1}(z)\rho_z F_z\tilde{z}\| \le \|e_i'B^{-1}(z)\rho_z\|\|F_z\tilde{z}\| \le \|e_i'B^{-1}(z_t)\|\|F_z\tilde{z}\|$$
$$\le (1 - \tau_i)\bar{u}_i \tag{A4}$$

Then, with Eqs. (24) and (A4),

$$|u_i| \le \|e_i'B^{-1}(z)\rho_z F_z\tilde{z}\| + \|e_i'B^{-1}(z)F_0(z)\| \le \bar{u}_i \tag{A5}$$
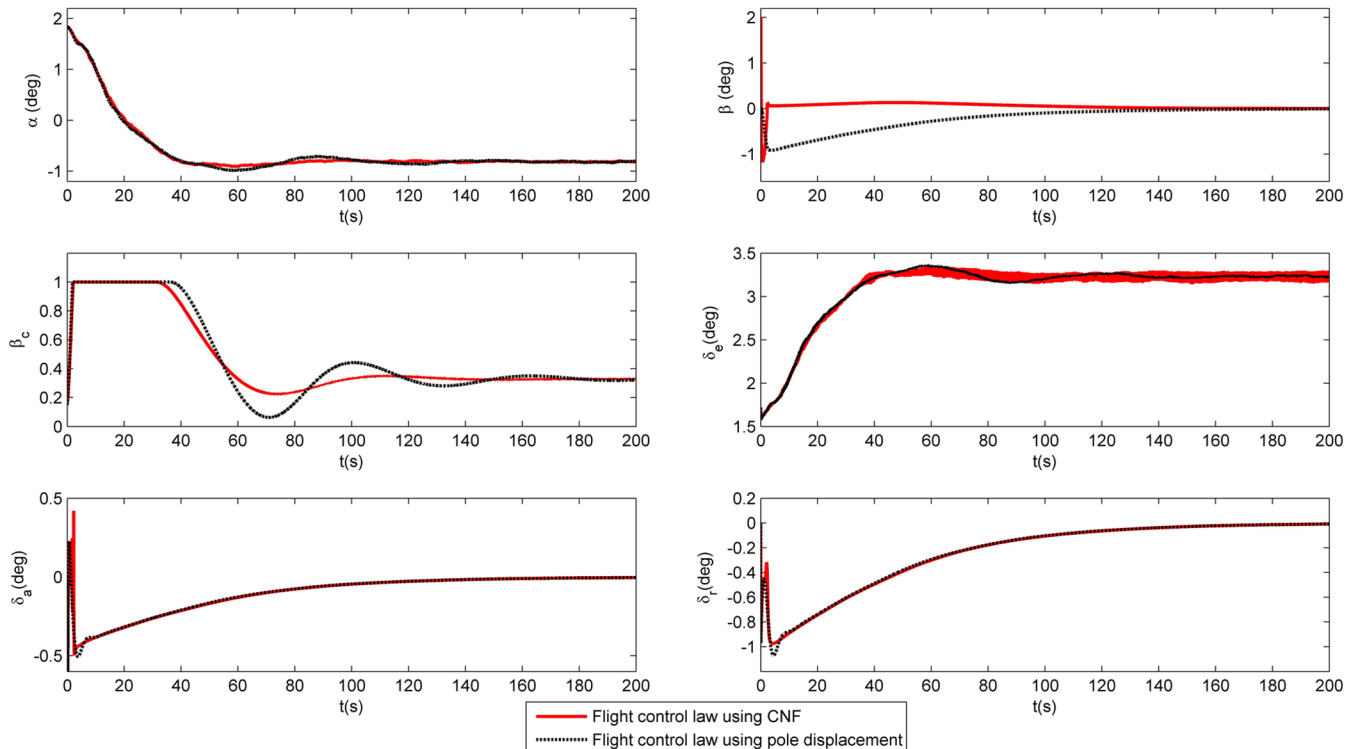
Fig. 6   Flight states and control inputs for uncertain model.

Thus,

$$[\text{sat}(u_V), \text{sat}(u_h)]' = B(z)^{-1}[\rho_z F_z(z - G_{ze}y_c) - F_0(z)] \quad (A6)$$

When $\|\rho_z\| > \sigma_{\min}(R_p) > 0$,

$$u_i = e_i' B^{-1}(z)\rho_z F_z \tilde{z} - e_i' B^{-1}(z)F_0(z)$$
$$r = e_i' B^{-1}(z)\tilde{\rho}_z F_z \tilde{z} + e_i' B^{-1}(z)[\rho_{z\sigma} F_z \tilde{z} - F_0(z)] \quad (A7)$$

where $\tilde{\rho}_z = \rho_z - \rho_{z\sigma}$ and $\rho_{z\sigma} = \text{diag}(\rho_{zV}, \rho_{zh}) - \varepsilon I$, where any of ρ_{zV} and ρ_{zh} is replaced with $\sigma_{\min}(R_p)$ if it is larger than $\sigma_{\min}(R_p)$ and ε is positive and near to zero introduced if necessary so that $\tilde{\rho}_z$ is invertible. Thus, $\|\rho_{z\sigma}\| < \sigma_{\min}(R_p)$ and

$$[\text{sat}(u_V), \text{sat}(u_h)]' = q_z B^{-1}(z)\tilde{\rho}_z F_z \tilde{z} + B^{-1}(z)[\rho_{z\sigma} F_z \tilde{z} - F_0(z)] \quad (A8)$$

where $q_z = \text{diag}(q_{zV}, q_{zh})$, and $q_{zV}, q_{zh} \in [0, 1]$. Finally, Eqs. (A6) and (A8) are integrated as

$$[\text{sat}(u_V), \text{sat}(u_h)]' = B(z)^{-1}[\bar{\rho}_z F_z(z - G_{ze}y_c) - F_0(z)] \quad (A9)$$

$$\bar{\rho}_z = \begin{cases} \rho_z & 0 < \|\rho_z\| \le \sigma_{\min}(R_p) \\ B(z)q_z B^{-1}(z)\tilde{\rho}_z + \rho_{z\sigma} & \|\rho_z\| > \sigma_{\min}(R_p) > 0 \end{cases} \quad (A10)$$

Accordingly, the closed-loop system comprising Eqs. (19) and (22) can be expressed by

$$\dot{\tilde{z}} = (A_z + B_z\bar{\rho}_z F_z)\tilde{z} \quad (A11)$$

To prove stability, we choose a Lyapunov function as

$$\Gamma_z = \tilde{z}' P_z \tilde{z} \quad (A12)$$

Then, the derivative of Γ_z can be computed along the direction of Eq. (A11) and with Eq. (15), and it is written by

$$\dot{\Gamma}_z = \dot{\tilde{z}}' P_z \tilde{z} + \tilde{z}' P_z \dot{\tilde{z}}$$
$$= \tilde{z}'[-Q_z + P_z B_z(R_z^{-1} - R_z^{-1}\bar{\rho}_z - \bar{\rho}_z R_z^{-1})B_z' P_z]\tilde{z} \quad (A13)$$

When $\|\rho_z\| \le \sigma_{\min}(R_p)$, we have

$$\dot{\Gamma}_z = -\tilde{z}' Q_z \tilde{z} + \tilde{z}' P_z B_z R_z^{-1}(I - 2\rho_z)B_z' P_z \tilde{z} \quad \le -\tilde{z}' Q_z \tilde{z} < 0 \quad (A14)$$

When $\|\rho_z\| \ge \sigma_{\min}(R_p)$, we have

$$\dot{\Gamma}_z = \tilde{z}'[-Q_z + P_z B_z(R_z^{-1} - R_z^{-1}\bar{\rho}_z - \bar{\rho}_z R_z^{-1})B_z' P_z]\tilde{z}$$
$$= -\tilde{z}' Q_z \tilde{z} + \tilde{z}' P_z B_z R_z^{-1}(I - 2\rho_{z\sigma})B_z' P_z \tilde{z}$$
$$- \tilde{z}' P_z B_z R_\rho[(p_\rho')^{-1}q_z p_\rho' + p_\rho q_z p_\rho^{-1}]R_\rho B_z' P_z \tilde{z} \quad (A15)$$

where, $R_\rho = (\tilde{\rho}_z R_z^{-1})^{1/2}$ and $p_\rho = R_\rho^{-1}B(z)$. Considering

$$\lambda_{\min}[(p_\rho')^{-1}q_z p_\rho' + p_\rho q_z p_\rho^{-1}] = 2\min(q_{zV}, q_{zh}) \quad (A16)$$

and with Eqs. (25), (A15), and (A16), we have

$$\dot{\Gamma}_z \le -\tilde{z}' Q_z \tilde{z} < 0 \quad (A17)$$

These imply that, once $\tilde{z} \in X_{iV}$, $\tilde{z}$ will never be out of X_{iV} and $\dot{\Gamma}_z < 0$ if Eqs. (24) and (25) are satisfied. Therefore, based on $\tilde{z} = z - G_{ze}y_c$, the system outputs can asymptotically track the step commands. Correspondingly, this completes the proof of Theorem 1.

References

[1] Braun, R. D., Wright, H. S., and Croom, M. A., "Design of the ARES Mars Airplane and Mission Architecture," *Journal of Spacecraft and Rockets*, Vol. 43, No. 5, 2006, pp. 1026–1034.
doi:10.2514/1.17956

[2] Li, S., and Jiang, X., "Review and Prospect of Guidance and Control for Mars Atmospheric Entry," *Progress in Aerospace Sciences*, Vol. 69, No. 4, 2014, pp. 40–57.
doi:10.1016/j.paerosci.2014.04.001

[3] Smith, S. C., Guynn, M. D., Streett, C. L., and Beeler, G. B., "Mars Airplane Airfoil Design with Application to ARES," *2nd AIAA "Unmanned Unlimited" Systems, Technologies, and Operations Conference*, AIAA Paper 2003-6607, Sept. 2003.

[4] Hjartarson, A., Paw, Y. C., and Chakraborty, A., "Modeling and Control Design for the ARES Aircraft," *AIAA Guidance, Navigation and Control Conference and Exhibit*, AIAA Paper 2008-7542, Aug. 2008.

[5] Bhattacharya, R., and Valasek, J., "On Modeling and Robust Control of ARES," *AIAA Guidance, Navigation and Control Conference and Exhibit*, AIAA Paper 2008-7454, Aug. 2008.

[6] Brown, N., Samuel, A., and Colgren, R., "Mars Exploration Airplane Design, Construction, and Flight Testing of a Stability, Control and Performance Demonstrator," *AIAA Infotech@Aerospace Conference and Exhibit*, AIAA Paper 2007-2723, May 2007.

[7] Ferreres, G., and Puyou, G., "Flight Control Law Design for a Flexible Aircraft: Limits of Performance," *Journal of Guidance, Control, and Dynamics*, Vol. 29, No. 4, 2006, pp. 870–878.
doi:10.2514/1.18535

[8] Chen, B. M., Lee, T. H., and Peng, K., "Composite Nonlinear Feedback Control for Linear Systems with Input Saturation: Theory and an Application," *IEEE Transactions on Automatic Control*, Vol. 48, No. 3, 2003, pp. 427–439.
doi:10.1109/TAC.2003.809148

[9] Peng, K., Chen, B. M., and Cheng, G., "Modeling and Compensation of Nonlinearities and Friction in a Micro Hard Disk Drive Servo System with Nonlinear Feedback Control," *IEEE Transactions on Control Systems Technology*, Vol. 13, No. 5, 2005, pp. 708–721.
doi:10.1109/TCST.2005.854321

[10] Restrepo, C., and Valasek, J., "Structured Adaptive Model Inversion Controller for Mars Atmospheric Flight," *Journal of Guidance, Control, and Dynamics*, Vol. 31, No. 4, 2008, pp. 937–953.
doi:10.2514/1.33085

[11] Liu, Y. B., Deng, J., and Lu, Y. P., "Preliminary Research on Optimal Design Based on Control Demands for Hypersonic Morphing Vehicle," *IEEE Aerospace and Electronic Systems Magazine*, Vol. 28, No. 5, 2013, pp. 23–31.
doi:10.1109/MAES.2013.6516146

[12] Sachs, G., and Moravszki, C., "Predictive Tunnel Display for Hypersonic Flight Path Control," *AIAA Guidance, Navigation, and Control Conference and Exhibit*, AIAA Paper 2006-6562, Aug. 2006.

[13] Sachs, G., "Increase and Limit of $T_\theta 2$ in Super- and Hypersonic Flight," *Journal of Guidance, Control, and Dynamics*, Vol. 22, No. 1, 1999, pp. 181–183.
doi:10.2514/2.7625

[14] Marrison, C. I., and Stengel, R. F., "Design of Robust Control Systems for a Hypersonic Aircraft," *Journal of Guidance, Control, and Dynamics*, Vol. 21, No. 1, 1998, pp. 58–63.
doi:10.2514/2.4197

[15] Wang, Q., and Stengel, R. F., "Robust Nonlinear Control of a Hypersonic Aircraft," *Journal of Guidance, Control, and Dynamics*,

Vol. 23, No. 4, 2000, pp. 577–585.
doi:10.2514/2.4580

[16] Xu, H., Mirmirani, M. D., and Ioannou, P. A., "Adaptive Sliding Mode Control Design for a Hypersonic Flight Vehicle," *Journal of Guidance, Control, and Dynamics*, Vol. 27, No. 5, 2004, pp. 829–838.
doi:10.2514/1.12596

[17] Peng, K., and Chen, B. M., "Variant Factor Technique for Tracking Control of a Class of Nonlinear Systems with Input Saturation," *Control and Intelligent Systems*, Vol. 41, No. 3, 2013, pp. 169–177.
doi:10.2316/Journal.201.2013.3.201-2506

[18] Valasek, J., Akella, M. R., Siddarth, A., and Rollins, E., "Adaptive Dynamic Inversion Control of Linear Plants with Control Position

Constraints," *IEEE Transactions on Control Systems Technology*, Vol. 20, No. 4, 2012, pp. 918–933.
doi:10.1109/TCST.2011.2159976

[19] Chang, Y. C., "Robust Tracking Control for Nonlinear MIMO Systems via Fuzzy Approaches," *Automatica*, Vol. 36, No. 10, 2000, pp. 1535–1545.
doi:10.1016/S0005-1098(00)00083-2

[20] Hu, H. J., Mirmirani, M., and Ioannou, P. A., "Robust Neural Adaptive Control of a Hypersonic Aircraft," *AIAA Guidance, Navigation, and Control Conference and Exhibit*, AIAA Paper 2003-5641, Aug. 2003.